Structural Engineering and Mechanics, *Vol. 48, No. 6 (2013) 809-822*
DOI: http://dx.doi.org/10.12989/sem.2013.48.6.809

Full-scale tests and analytical model of the Teflon-based lead rubber isolation bearings

Lu Wang*, Jin Ou[a], Weiqing Liu[b] and Shuguang Wang[c]

College of Civil Engineering, Nanjing University of Technology, Nanjing, China

(Received July 22, 2013, Revised November 9, 2013, Accepted November 11, 2013)

Abstract. Base isolation is widely used in seismic resisting buildings due to its low construction cost, high reliability, mature theory and convenient usage. However, it is difficult to design the isolation layer in high-rise buildings using the available bearings because high-rise buildings are characterized with long period, low horizontal stiffness, and complex re-distribution of the internal forces under earthquake loads etc. In this paper, a simple and innovative isolation bearing, named Teflon-based lead rubber isolation bearing, is developed to address the mentioned problems. The Teflon-based lead rubber isolation bearing consists of friction material and lead rubber isolation bearing. Hence, it integrates advantages of friction bearings and lead rubber isolation bearings so that improves the stability of base isolation system. An experimental study was conducted to validate the effectiveness of this new bearing. The effects of vertical loading, displacement amplitude and loading frequency on the force-displacement relationship and energy dissipation capacity of the Teflon-based lead rubber isolation bearing were studied. An analytical model was also proposed to predict the force-displacement relationship of the new bearing. Comparison of analytical and experimental results showed that the analytical model can accurately predict the force-displacement relationship and elastic shear deflection of the Teflon-based lead rubber isolation bearings.

Keywords: teflon-based lead rubber isolation bearing; force-displacement relationship; bearing testing; restoring force; analytical model

1. Introduction

In recent years, base isolation technique has been considered to be an efficient approach for mitigating the seismic damage for buildings, bridges and equipments due to its advantages of low cost, high reliability, mature theory and convenient usage. There are two important base isolation systems, namely elastomeric isolation systems such as natural rubber bearings (NRB), lead rubber bearings (LRB) and high-damping rubber bearings (HDRB), and sliding isolation systems such as friction pendulum bearings (FPB) and Teflon bearings (TB).

A number of experimental and theoretical studies have been conducted to investigate the characteristics of rubber bearings (Hwang *et al.* 2002, Tsai *et al.* 2003, Yoshida *et al.* 2004). Abe

*Corresponding author, Ph.D., E-mail: kevinlwang@hotmail.com
[a]Professor, E-mail: oujin@njut.edu.cn
[b]Professor, E-mail: wqliu@njut.edu.cn
[c]Professor, E-mail: 720108@vip.sina.com

http://www.techno-press.org/?journal=sem&subpage=8 ISSN: 1225-4568 (Print), 1598-6217 (Online)

et al. (2004a) studied restoring force, equivalent stiffness and damping ratio of three types of laminated rubber bearings, including high-damping rubber bearing, natural rubber bearing and lead rubber bearing, under multiaxial loading state. All bearings were laminated with seven rubber layers and six inner steel plates. The test results showed that the effects of vertical loading on stiffness and damping ratio of LRBs under small deformation were much more serious than that of HDRBs and NRBs. Meanwhile, in triaxial loading test, the equivalent stiffness and damping ratio of HDRBs and NRBs increased due to the coupling effect in comparison with the biaxial loading case, while the LRBs showed a slight decrease in them. Hence, Abe et al. pointed that the coupling effect should be considered in designing seismic isolation of buildings with laminated rubber bearings. Furthermore, Abe *et al.* (2004b) proposed a two-dimensional model to predict the bidirectional horizontal behaviours of the bearings under a constant vertical load based on the three-dimensional constitutive law of the Ozdemir model. The analytical results agreed well with the test results of three types of bearings under triaxial loading conditions. To investigate the nonlinear behaviour of HDRBs, Yamamoto *et al.* (2009) conducted full scale tests of HDRBs under horizontal bidirectional loading. The test results indicated that the maximum restoring force in the direction orthogonal to the primary direction of loading occurred near zero displacement. Furthermore, based on the measured bearing restoring forces, Yamamoto *et al.* (2012) developed a rate-independent model, which can accurately predict the test results for both bidirectional and unidirectional loading, and describe the observed irregular restoring force characteristics around zero displacement. Although the cyclic behaviour of laminated rubber bearings and corresponding analytical models have been studied thoroughly, the effects of corrosion, fatigue and creep of rubber material on the cyclic behaviour of rubber bearings have not been effectively resolved. Furthermore, the natural rubber is a kind of temperature-dependent material, hence, the energy dissipation capacity of the rubber bearing is affacted by temperature.

In the past three decades, many studies have been conducted to investigate the cyclic behaviour of Teflon-stainless steel sliding isolation bearings (Hwang *et al*. 1990, Mokha *et al*. 1991, 1993, Constantinou *et al*. 1990) and friction pendulum bearings (Fenz *et al.* 2006, Yurdakul and Ates 2011, Ates 2012). Fenz (2008) investigated the force-displacement relationships of three types of sliding isolation bearings, involving triple friction pendulum bearing, the modified single friction pendulum bearing and double friction pendulum bearing. The corresponding analytical model based on equilibrium and geometry was proposed. The analytical results agreed well with the experimental testing results. Mosqueda (2004) examined the behaviour of friction pendulum bearings under bi-directional loading. The force-displacement relationships and friction coefficient were studied. Becker and Mahin (2012) developed a kinematic model to describe the bi-directional behaviour of the triple friction pendulum bearing according to geometric compatibility relationships of the bearing components. The tests results revealed that the analytical model can accurately predict the normalized shear and displacement of bearings. However, some disadvantages of sliding bearings cannot be ignored. First, the horizontal stiffness of high-rise buildings are relatively low, but the horizontal stiffness of sliding isolation bearings are also nearly infinite before sliding, which are incompatibility with high-rise buildings and other laminated rubber bearings; Second, because the sliding isolation bearings cannot deform back to the original position by themselves, the large sliding displacement under strong earthquake could lead to instability problems for the building. Hence, sliding isolation bearings should be arranged in the isolation layer combined with other bearings or dampers.

To overcome several of the aforementioned shortcomings, it is necessary to develop a new isolation bearing which can integrate advantages of existing bearings to mitigate the seismic

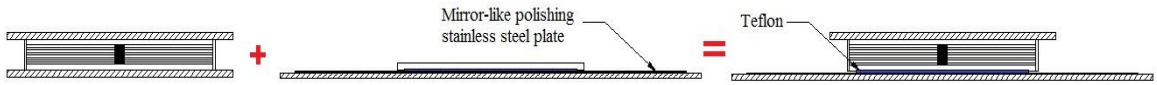

Lead rubber bearing | Teflon-stainless steel sliding bearing isolation bearing | Teflon-Based lead rubber

Fig. 1 Construction of Teflon-based lead rubber isolation bearing

damage for structures. Recently, combining natural rubber bearing and shape memory alloy (SMA) in seismic isolation have been studied (Hedayati and Shahria 2013, Bhuiyan *et al*. 2013). Although the shape memory alloy-based laminated rubber isolation bearing can partially solve the problems incurred by laminated rubber bearings, the usage amount is restricted by the high cost of shape memory alloy. Hence, an innovation isolation bearing, named Teflon-based lead rubber isolation bearing (TLRB), is developed with simple construction and low cost in this paper. The TLRB, as shown in Fig. 1, consists of top and bottom steel plates, lead rubber isolation bearing (LRB), friction material (Teflon) and a mirror-like polishing stainless steel plate. The LRB and Teflon are combined into an entirety under high temperature and high pressure. Teflon is chosen as the friction material due to the low coefficient of friction, excellent endurance against fatigue and corrosion resistance. The mirror-like polishing stainless steel plate and Teflon are used on sliding interface. The functions of LRB are to adjust the initial horizontal and vertical stiffnesses of TLRB, and potentially recover the residual deformations after the earthquake. Once TLRB starts sliding, the horizontal stiffness of TLRB becomes zero, which could be beneficial to extending the period of structures. In the meantime, the use of the sliding bearing can weaken the influence of temperature on the energy dissipation capacity. Because TLRB overcomes the disadvantages of friction bearings and lead rubber isolation bearings, the stability of base isolation system can be enhanced significantly. An experimental study was conducted to validate the effectiveness of this new bearing. An analytical model was developed to describe the force-displacement relationship of TLRB.

2. Experimental program

2.1 Description of test specimens

In this study, three full-scale TLRBs were fabricated and tested. The details of TLRB are shown in Fig. 2. All the specimens had the same dimensions. For the LRB, the diameters of steel shim and rubber layer were 600 mm. The thicknesses of steel shim and rubber layer were 3 mm and 4 mm, respectively. The numbers of steel shim and rubber were 4 layers and 5 layers, respectively. The diameter of lead core was 20 mm. The height of LRB was 88 mm. The thickness of rubber protection layer was 20 mm. For the Teflon, the diameter and thickness were 560 mm and 6 mm, respectively, as shown in Fig. 3. The thickness of Teflon embedded into the LRB was 3 mm. The thickness of top and bottom steel plates were 20 mm and 25 mm, respectively. The size of mirror-like polishing stainless steel plate was 1380 mm × 1380 mm × 5 mm. The material properties of steel plates and rubber are summarized in Tables 1-2.

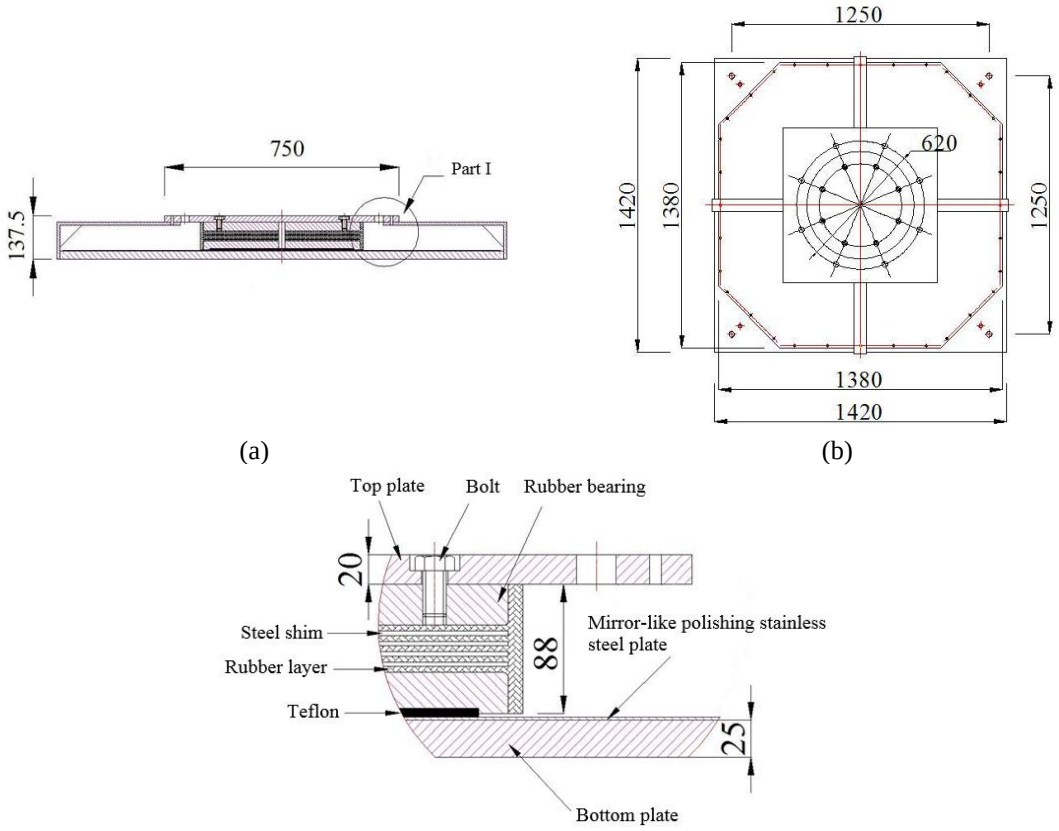

Fig. 2 The schematic diagram of the Teflon-based lead rubber isolation bearing: (a) elevation view, (b) plan view and (c) details of part I

Table 1 Material properties of steel plates

	t_p (mm)	f_{yp} (MPa)	E_p (GPa)
Steel shim	3	321	215
Top plates	20	315	205
Bottom plates	25	317	209
Mirror-like stainless steel plate	5	296	590

Table 2 Material properties of rubber

Type	*HS*	f_t (MPa)	ξ_u (%)	T_b (℃)
Natural rubber	61	17	450	-60

2.2 Test set-up and instrumentation

As shown in Fig. 4, the base of the hydraulic servo loading system was bolted to the strong floor of the laboratory. The system consisted of four vertical actuators and two horizontal actuators

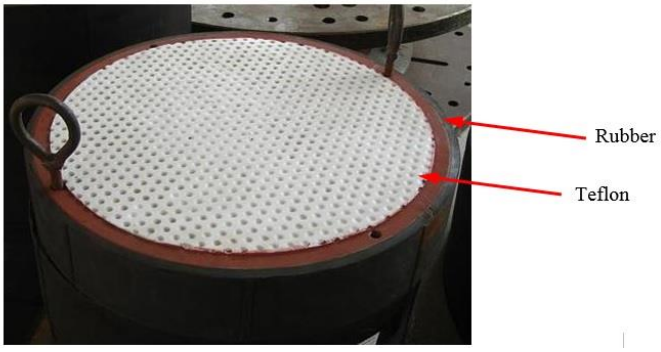

Fig. 3 Construction of Teflon-based lead rubber isolation bearing

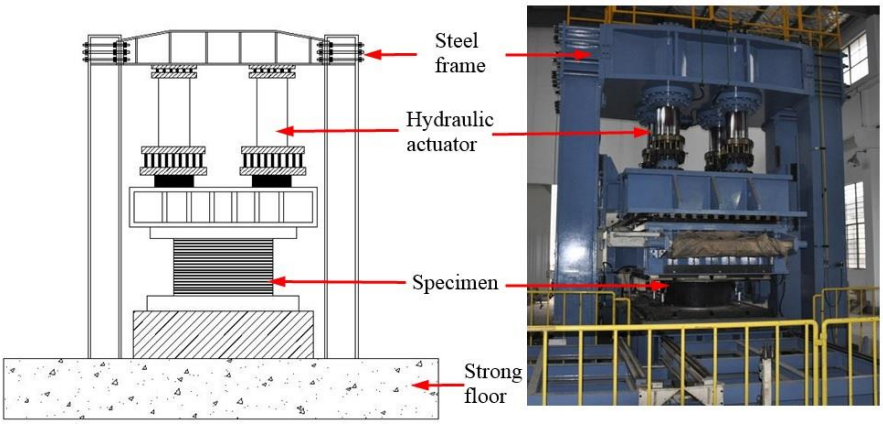

(a) (b)

Fig. 4 Test setup: (a) schematic diagram and (b) photograph of the test setup

which transmitted loads to the bearing via a thick flange plate. The top and bottom steel plates of TLRB were connected to the flange and base plates of loading system, respectively. Vertical loading was applied by vertical hydraulic actuators with a loading capacity of 20000 kN. The vertical actuators were force-controlled to accommodate changes in the bearing's height while still maintaining a constant vertical compression loading. Horizontal force was applied by horizontal hydraulic actuators with a loading capacity of 6000 kN and displacement amplitude of 800 mm. The horizontal actuators were displacement-controlled and imposed a predefined displacement history.

Horizontal and vertical loading data were collected by a five-channel load cell that was mounted directly beneath the TLRB. Horizontal displacement was measured by four linear variable displacement transducers (LVDTs) which were internal to the horizontal actuator. The displacement data was the total displacement of the top steel plate of the bearing with respect to the bottom steel plate.

2.3 Test procedure

The aim of testing is to evaluate the force-displacement relationship and study the effects of

Table 3 Experimental cases of Teflon-based lead rubber isolation bearings

Specimen	Case	P (kN)	d (mm)	F (Hz)	Cycle
TLRB1	SB1	3000	200	0.0039	3
TLRB1	SB2	3000	300	0.0039	3
TLRB1	SB3	3000	400	0.0039	3
TLRB2	SB4	2000	300	0.0039	3
TLRB2	SB5	4000	300	0.0039	3
TLRB3	SB6	3000	200	0.0010	3
TLRB3	SB7	3000	200	0.0079	3

vertical loading, displacement amplitude and loading frequency on the energy dissipation capacity and friction performance of TLRB. There were totally seven test cases according to different loading conditions. Specimen TLRB1 was used to conduct Case SB1 to Case SB3, Specimen TLRB2 was used to conduct Case SB4 and Case SB5, and Specimen TLRB3 was used to conduct Case SB6 and Case SB7. All tests were conducted under a constant vertical loading with three fully reversed cycles of horizontal displacement. The vertical loading, displacement amplitude and loading frequency of each of the test cases are listed in Table 3. Prior to every test, to weaken the effects of contamination on the coefficient of friction, the interface of mirror-like polishing stainless steel plate was cleaned with alcohol and a soft cloth. Meanwhile, to avoid uneven vertical loading on the bearings, the bearings should be centred within the loading system before testing.

3. Test results and evaluation

3.1 Relationship between vertical loading and restoring force

Fig. 5(a) illustrates the effects of axial compression loading (P) on the dynamic behaviour of ESB. For Case SB5, the restoring force of TLRB with P = 4000 kN was 89 kN, which was much larger than those of Case SB2 (61 kN) with P = 3000kN and Case SB4 (48 kN) with P = 2000 kN under the same displacement amplitude (d = 300 mm) and loading frequency (f = 0.0039 Hz), respectively. Furthermore, the area enclosed by a hysteresis loop of Case SB5 was roughly 45.9% and 85.4% larger than those of Case SB2 and Case SB4, respectively, which means that the energy dissipation capacity of Case SB5 was much larger than those of Case SB2 and Case SB4. Therefore, increasing vertical loading on the TLRB leads to greater restoring force and energy dissipation capacity under the same displacement amplitude and loading frequency.

3.2 Relationship between displacement amplitude and restoring force

Fig. 5(b) illustrates the effects of displacement amplitude on the force-displacement relationship of TLRB. For Case SB3, the restoring force of TLRB was 63 kN with d = 400 mm, which was generally the same as those of Case SB1 (60 kN) with d = 200 mm and Case SB2 (61 kN) with d = 300 mm under the same vertical loading (P = 3000 kN) and loading frequency (f = 0.0039 Hz). However, the area enclosed by a hysteresis loop of Case SB3 was roughly 110.0% and 37.7% larger than those of Case SB1 and Case SB2, respectively, which indicates that the energy

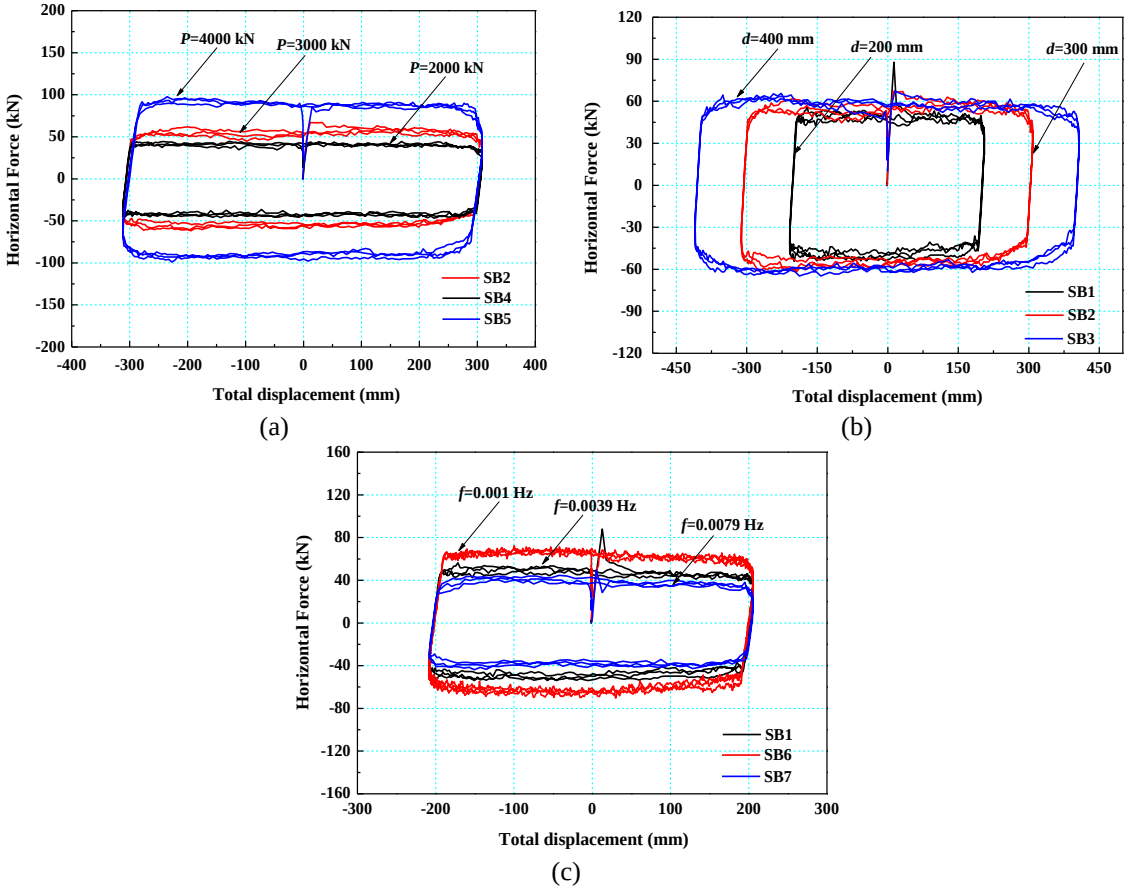

Fig. 5 Force-displacement relationship: (a) effects of vertical loading, (b) effects of displacement amplitude and (c) effects of loading frequency

dissipation capacity of Case SB3 was much larger than those of Case SB2 and Case SB3. The results prove that the energy dissipation capacity of TLRB was affected by the displacement amplitude significantly, and a larger displacement amplitude can give a higher energy dissipation capacity. Meanwhile the restoring force of TLRB kept stable under the same vertical loading and loading frequency.

3.3 Relationship between loading frequency and restoring force

Fig. 5(c) illustrates the effects of loading frequency on the force-displacement relationship of TLRB. For Case SB6, the restoring force of TLRB with f = 0.001 Hz was 69 kN, which was larger than those of Case SB1 (60 kN) with f = 0.0039 Hz and Case SB7 (49 kN) with f = 0.0079 Hz under the same vertical loading (P = 3000 kN) and displacement amplitude (d = 300 mm), respectively. Furthermore, the area enclosed by a hysteresis loop of Case SB6 was roughly 15.0% and 40.8% larger than those of Case SB1 and Case SB7, respectively, which reveals that the energy dissipation capacity of Case SB6 was larger than those of Case SB1 and Case SB7. The results demonstrate that the restoring force of TLRB was affected by the loading frequency. A

larger loading frequency can lead to a smaller maximum damping force and energy dissipation capacity under the same vertical loading and displacement amplitude.

3.4 Equivalent horizontal stiffness and damping ratio

For the bearings, the equivalent stiffness K_{eq} and damping ratio ζ_{eq} can be obtained with the following equations (Chopra 1995)

$$K_{eq} = \frac{F_{\max}}{U_{\max}} \tag{1}$$

$$\varsigma_{eq} = \frac{1}{4\pi}\left(\frac{\Delta W}{W_e}\right) \tag{2}$$

where U_{max} is the maximum absolute displacement in a loop; F_{max} is absolute force value at the displacement U_{max}; ΔW is area enclosed by the hysteretic loop; and W_e is elastic potential energy defined at displacement U_{max}.

The equivalent stiffness and damping ratio for different test cases are summarized in Table 4. Figs. 6(a) and (b) show the effects of vertical loading on the equivalent horizontal stiffness and damping ratio, respectively. For Case SB5, the equivalent horizontal stiffness with P = 4000 kN was 0.30 kN/mm, which was larger than those of Case SB2 (0.20 kN/mm) with P = 3000kN and Case SB4 (0.16 kN/mm) with P = 2000kN under the same displacement amplitude (d = 300 mm) and loading frequency (f = 0.0039 Hz), respectively. Meanwhile, the damping ratio for Case SB4 was 0.76, which was much smaller than those of Case SB2 and Case SB5. Thus, the larger vertical loading on the bearings can lead to larger equivalent horizontal stiffness and smaller damping ratio under the same displacement amplitude and loading frequency.

Figs. 7(a) and (b) show the effects of loading frequency on the equivalent horizontal stiffness and damping ratio, respectively. Under the condition of P = 3000 kN and d = 300 mm, the largest equivalent horizontal stiffness and damping ratio were 0.35 kN/mm and 1.37 (Case SB6, f = 0.001 Hz), and the smallest equivalent horizontal stiffness and damping ratio were 0.25 kN/mm and 0.73 (Case SB7, f = 0.0079 Hz). Thus, the test results demonstrated that increasing loading frequency leads to smaller equivalent horizontal stiffness and damping ratio under the same vertical loading and displacement amplitude.

Table 4 Experimental and analytical results of Teflon-based lead rubber isolation bearings

Case	K_{eq} (kN/mm)	ζ_{eq}	F (kN)	$F^{'}$ (kN)	$F / F^{'}$
SB1	0.30	1.10	60	59	1.05
SB2	0.20	0.89	61	59	1.02
SB3	0.16	0.78	63	59	1.03
SB4	0.16	0.76	48	43	1.12
SB5	0.30	1.01	89	85	1.05
SB6	0.35	1.37	69	62	1.11
SB7	0.25	0.73	49	48	0.98
Mean	-	-	-	-	1.05

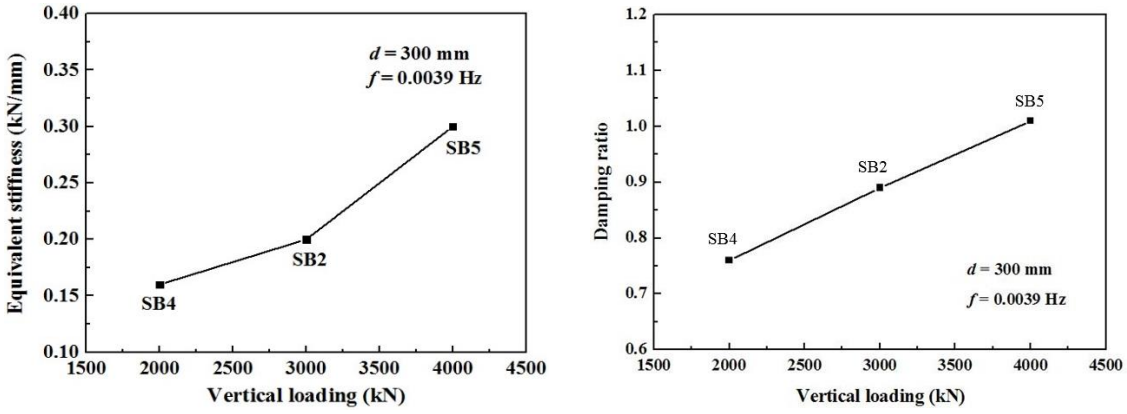

(a) (b)

Fig. 6 Effects of vertical loading: (a) equivalent horizontal stiffness and (b) damping ratio

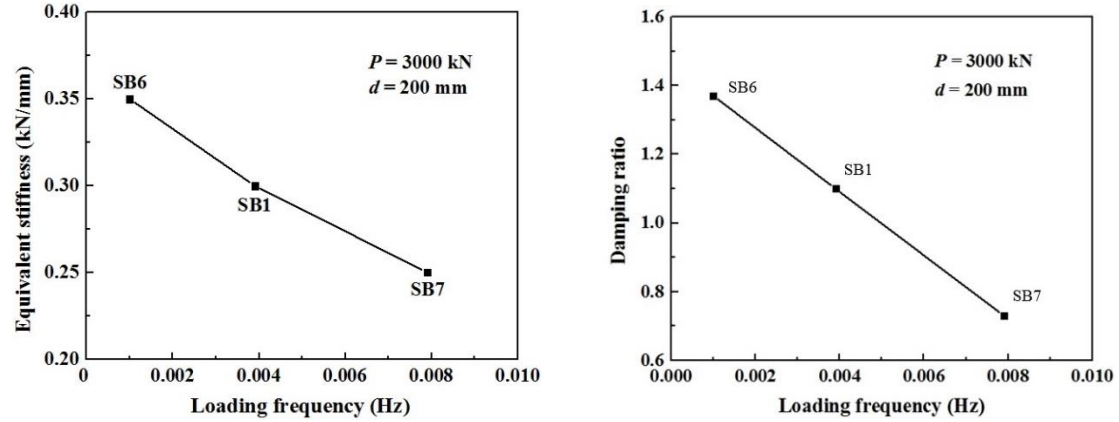

(a) (b)

Fig. 7 Effects of loading frequency: (a) equivalent horizontal stiffness and (b) damping ratio

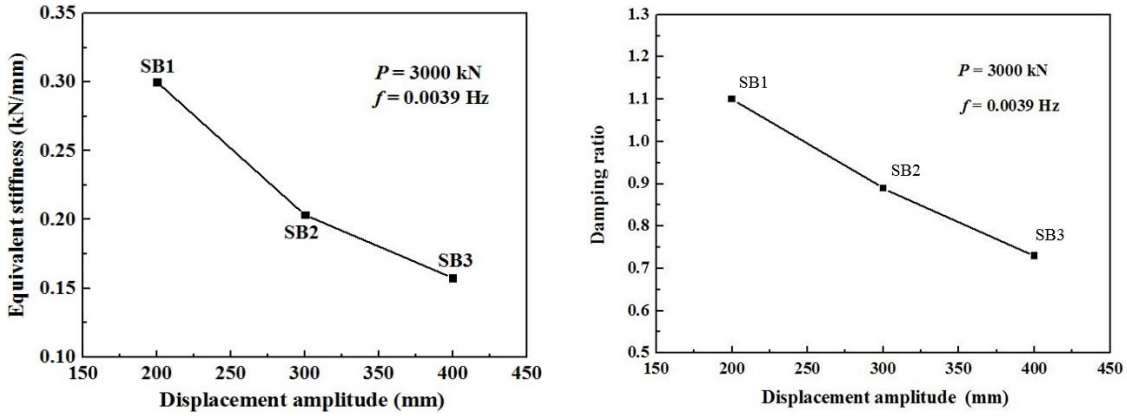

(a) (b)

Fig. 8 Effects of displacement amplitude: (a) equivalent horizontal stiffness and (b) damping ratio

Figs. 8(a) and (b) show the effects of displacement amplitude on the equivalent horizontal stiffness and damping ratio, respectively. For Case SB1, the equivalent horizontal stiffness and with d = 200 mm was 0.30 kN/mm, which was 47.5% and 90.5% larger than those of Case SB2 with d = 300 mm and Case SB3 with d = 400 mm under the same vertical loading (P = 3000 kN) and loading frequency (f = 0.0039 Hz), respectively. Meanwhile, the damping ratio for Case SB1 was 1.10, which was 23.6% and 41.0% larger than those of Case SB2 and Case SB3. Therefore, the equivalent horizontal stiffness and damping ratio can be smaller with increase in displacement amplitude under the same vertical loading and loading frequency.

4. Analytical model

4.1 Friction models

A large number of friction models have been studied by researchers in the past years, which can be divided into two types: non-continuous friction (NCF) model and continuous friction (CF) model. For the NCF models, the friction was expressed with piecewise functions, such as coulomb friction model and explosion friction model as shown in Fig. 9(a); for the CF models, the friction was the smooth continuous function of sliding velocity, such as continuous explosion friction model and equivalent viscous damping model. However, no matter each of friction model cannot predict the initial horizontal stiffness and elastic shear deflection of TLRB.

4.2 Bilinearity-Explosion friction-Ramberg Osgood model

To address the above shortcomings, an innovative friction model, named Bilinearity-Explosion friction-Ramberg Osgood (BER) model (see Fig. 9(c)), was proposed to predict the force-displacement relationship of TLRB. BER model consistes of explosion friction model and Bilinearity-Ramberg Osgood model. Because Bilinearity-Ramberg Osgood model, as shown in Fig. 9(b), can predict the elastic shear deflection of rubber bearing, the BER model is much accurately to describe the force-displacement relationship of TLRB than explosion friction model.

For Segment AB, the restoring force (F) of TLRB is

$$F=K_1x \qquad (0\leq x\leq x_y) \tag{3}$$

where x is the horizontal displacement, x_y is the horizontal yield displacement, and K_1 is the initial stiffness of TLRB.

For Segments BC, DE and FB, because the elastic shear deflection of laminated rubber bearing is nearly stable when the bearing begins sliding, the restoring force can be calculated according to the explosion friction model

$$F = \mu(x_0^{'})sign(x_0^{'}, x_g^{'})P \tag{4}$$

where $x_0^{'}$ and $x_g^{'}$ are the velocities of isolation layer and ground motion, respectively, *sign* is the sign function, P is the axial vertical loading, and function μ can be expressed as

$$\mu(x_0^{'}) = a + be^{-d\left|x_0^{'}\right|} \tag{5}$$

where a, b and d are constants, which can be determined from test results

$$sign(\dot{x}_0, \dot{x}_g) = \begin{cases} -sign(\dot{x}_0) & \dot{x}_0 \neq 0 \\ sign(\dot{x}_0) & \dot{x}_0 \neq 0 \end{cases} \tag{6}$$

For Segments CD and EF, the restoring force can be expressed as Eq. (7)

$$(F-F_u) = (x-x_u)/(m+n|F-F_u|^{r-1}) \tag{7}$$

where F_u is the ultimate loading, r is constant determined from test results, and m and n are constants which can be calculated by Eqs. (8)-(9), respectively.

$$m = \frac{1}{k_u} \tag{8}$$

$$n = \frac{1}{\left|F_t - F_u\right|^{r-1}}\left(\frac{1}{K_t} - \frac{1}{K_u}\right) \tag{9}$$

where K_t and K_u are the tangent stiffness and ultimate stiffness of TLRB, respectively, which can be determined from test results, and F_t is the restoring loading at Point D, as shown in Fig. 9(c).

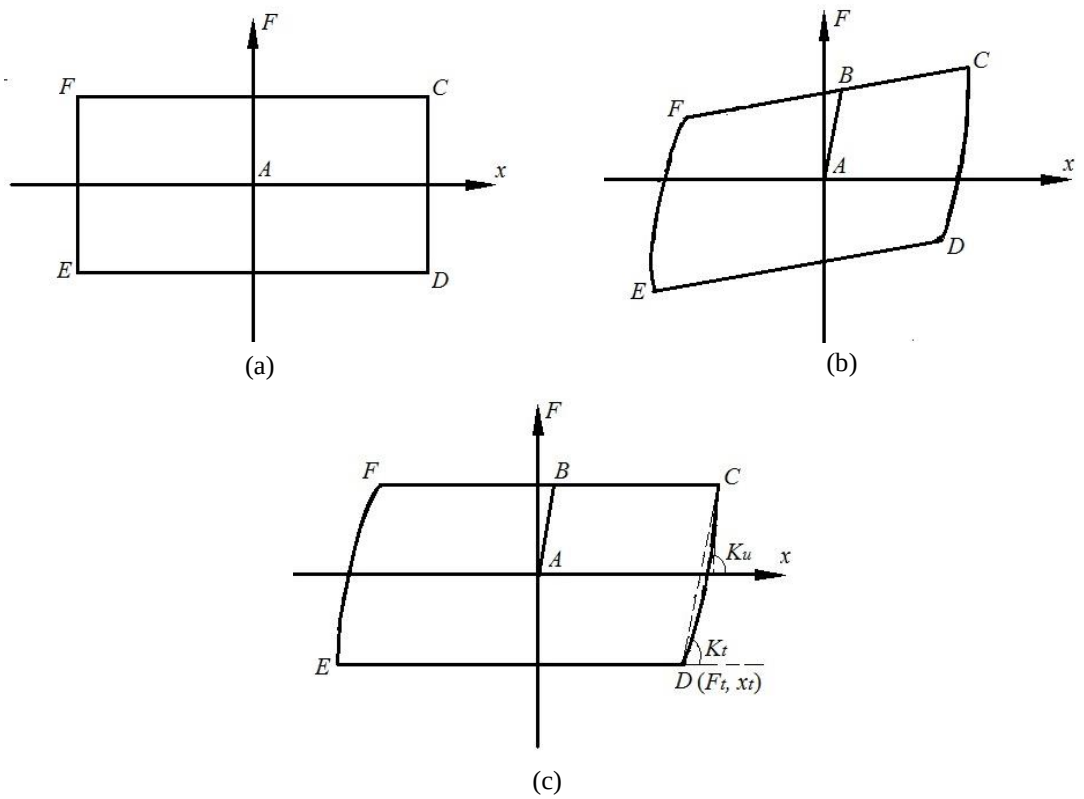

Fig. 9 Analytical model: (a) Explosion friction model; (b) Bilinearity-Ramberg Osgood model and (c) Bilinearity-explosion friction-Ramberg Osgood model

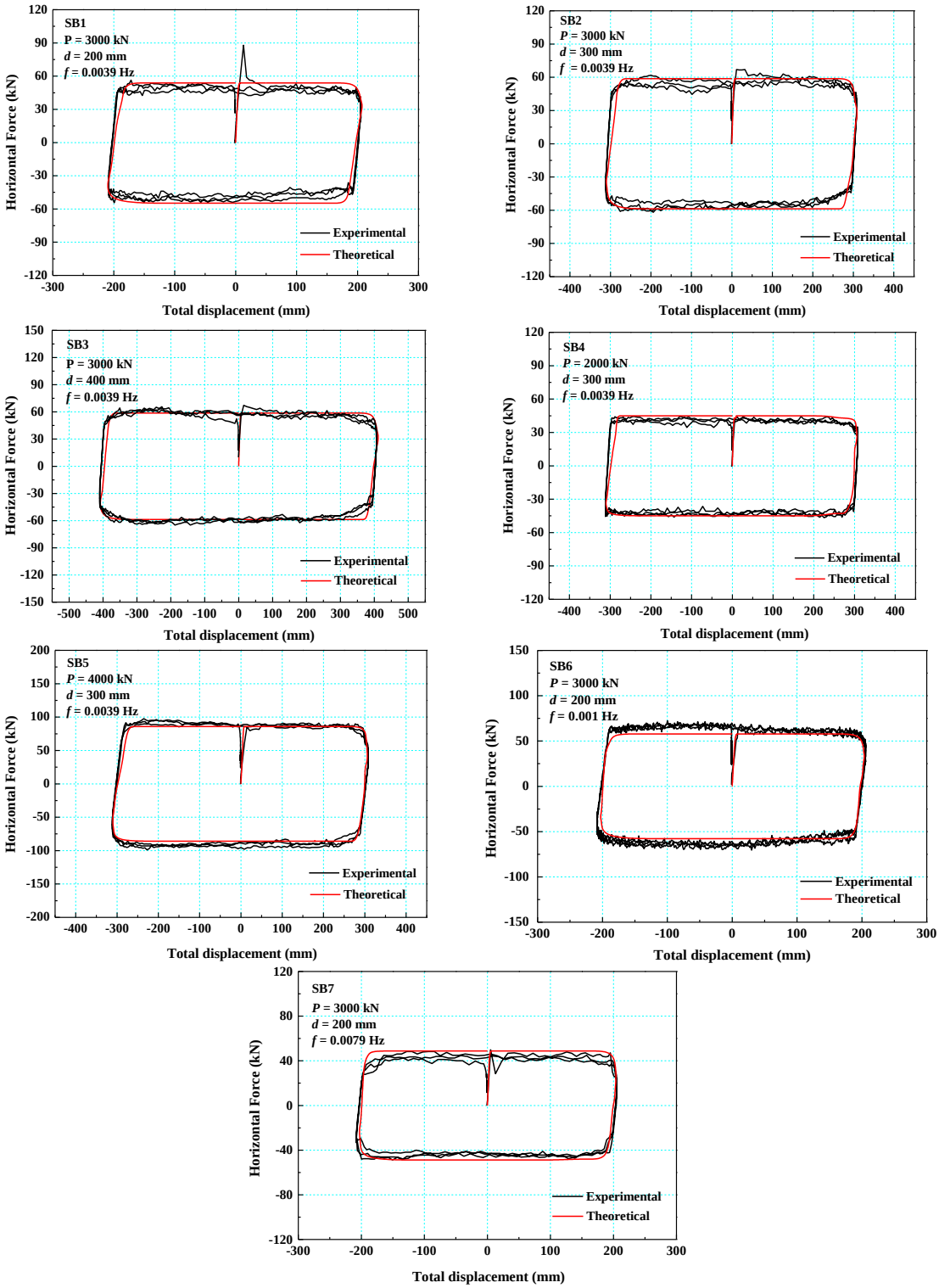

Fig. 10 Comparison of analytical and experimental results for force–displacement relationship

4.3 Comparison of experimental and analytical results

Using Eqs. (3)-(7), the force-displacement relationships of TLRB under different test cases were evaluated. The comparison between predicted and experimental force-displacement relationships are shown in Fig. 10. Comparing the analytical and experimental restoring forces reveals that the analytical model is generally able to conservatively estimate the restoring force of TLRB with an average underestimation of 5%.

5. Conclusions

The paper presents a study on the hysteretic restoring force characteristics and analytical model of the Teflon-based lead rubber isolation bearings. The analytical and experimental findings are summarized as follows:

(1) The experimental results show that the Teflon-based lead rubber isolation bearings have strong energy dissipation capacity. The initial horizontal stiffness is determined by lead rubber isolation bearings.

(2) The larger vertical load-carrying capacity and the smaller loading frequency on the bearings lead to greater damping force, while the changes of damping force under different displacement amplitude is slight.

(3) A larger vertical load-carrying capacity and displacement amplitude can give a higher energy dissipation capacity significantly.

(4) The larger vertical load-carrying capacity on the bearings can lead to larger equivalent horizontal stiffness and smaller damping ratio, while increasing loading frequency and displacement amplitude can lead to smaller equivalent horizontal stiffness and damping ratio.

(5) The Bilinearity-Explosion friction-Ramberg Osgood model was developed. The experimental and analytical results showed a good agreement with each other. This study demonstrates that the analytical model is able to accurately predict the force-displacement relationship and restoring force characteristics of the Teflon-based lead rubber isolation bearings.

Acknowledgments

The research described here was supported by the Key Program of National Natural Science Foundation of China (Grant No. 51238003), National Natural Science Foundation of China (Grant No. 50608039), and National Natural Science Foundation of China (Grant No. 51208023).

References

Fenz, D.M. and Constantinou, M.C. (2008), "Spherical sliding isolation bearings with adaptive behavior: Theory", *Earthq. Eng. Struct. Dyn.*, **37**(2), 163-183.

Fenz, D.M. and Constantinou, M.C. (2008), "Spherical sliding isolation bearings with adaptive behavior: Experimental verification", *Earthq. Eng. Struct. Dyn.*, **37**(2), 185-205.

Fenz, D.M. and Constantinou, M.C. (2006), "Behaviour of the double concave Friction Pendulum bearing", *Earthq. Eng. Struct. Dyn.*, **35**(11), 1403-1424.

Bhuiyan, A.R. and Alam, M.S. (2013), "Seismic performance assessment of highway bridges equipped with

superelastic shape memory alloy-based laminated rubber isolation bearing", *Eng. Struct.*, **49**, 396-407.
Hedayati, D.F. and Shahria, A.M. (2013), "Shape memory alloy wire-based smart natural rubber bearing", *Smart Mater. Struct.*, **22**(4), 1-17.
Hwang, J.S., Wu, J.D., Pan, T.C. and Yang, G. (2002), "A mathematical hysteretic model for elastomeric isolation bearings", *Earthq. Eng. Struct Dyn.*, **31**(4), 771-789.
Mokha, A., Constantinou, M. and Reinhorn, A. (1991), "Further results on frictional properties of Teflon bearings", *J. Struct. Eng*., ASCE, **117**(2), 622-626.
Mokha, A., Constantinou, M. and Reinhorn, A. (1993), "Verification of friction model of Teflon bearings under triaxial load", *J. Struct. Eng*., ASCE, **119**(1), 240-261.
Constantinou, M., Mokha, A. and Reinhorn, A. (1990), "Teflon bearings in base isolation. II: modeling", *J. Struct. Eng*., ASCE, **116**(2), 455-474.
Hwang, J.S., Chang, K.C. and Lee, G.C. (1990), "Quasi-static and dynamic sliding characteristics of Teflon stainless steel interfaces", *J. Struct. Eng*., ASCE, **116**(10), 2747-2762.
Mosqueda, G., Whittaker, A.S. and Fenves, G.L. (2004), "Characterization and modeling of friction pendulum bearings subjected to multiple components of excitation", *J. Struct. Eng*., ASCE, **130**(3), 433-442.
Ates, S. (2012), "Investigation of effectiveness of double concave friction pendulum bearings", *Comput Concrete*, **9**(3), 195-214.
Yurdakul, M. and Ates, S. (2011), "Modeling of triple concave friction pendulum bearings for seismic isolation of buildings", *Struct. Eng. Mech.*, **40**(3), 315-334.
Abe, M., Yoshida, J. and Fujino, Y. (2004a), "Multiaxial behaviors of laminated rubber bearings and their modeling. I: experimental study", *J. Struct. Eng*., ASCE, **130**(8), 1119-1132.
Abe, M., Yoshida, J. and Fujino, Y. (2004b), "Multiaxial behaviors of laminated rubber bearings and their modeling. II: modeling", *J. Struct. Eng*., ASCE, **130**(8), 1133-1144.
Yamamoto, S., Kikuchi, S., Ueda, M. and Aiken, I.D. (2009), "A mechanical model for elastomeric seismic isolation bearings including the influence of axial load", *Earthq. Eng. Struct. Dyn.*, **38**(2), 157-180.
Tsai, C.S., Chiang, T.C., Chen, B.J. and Lin, S.B. (2003), "An advanced analytical model for high damping rubber bearings", *Earthq. Eng. Struct. Dyn.*, **32**(9), 1373-1387.
Yoshida, J., Abe, M. and Fujino, Y. (2004), "Constitutive model of high-damping rubber materials", *J. Struct. Eng*., ASCE, **130**(2), 129-141.
Becker, T.C. and Mahin, S.A. (2012), "Experimental and analytical study of the bi-directional behaviour of the triple friction pendulum isolator", *Earthq. Eng. Struct. Dyn.*, **41**(3), 355-373.
Yamamoto, M., Minewaki, S., Yoneda, H. and Higashino, M. (2012), "Nonlinear behavior of high-damping rubber bearings under horizontal bidirectional loading: full-scale tests and analytical modeling", *Earthq. Eng. Struct. Dyn.*, **41**(13), 1845-1860.